The International Journal of Advanced Manufacturing Technology (2024) 130:2833–2845
https://doi.org/10.1007/s00170-023-12826-8

ORIGINAL ARTICLE

# Optimisation of process parameters for improving surface quality in laser powder bed fusion

Yuchu Qin[1] · Shan Lou[1] · Peizhi Shi[2] · Qunfen Qi[3] · Wenhan Zeng[1] · Paul J. Scott[1] · Xiangqian Jiang[1]

Received: 4 September 2023 / Accepted: 1 December 2023 / Published online: 21 December 2023
© The Author(s) 2023

**Abstract**
Surface quality is one of the critical factors that affect the performance of a laser powder bed fusion part. Optimising process parameters in process design is an important way to improve surface quality. So far, a number of optimisation methods have been presented within academia. Each of these methods can work well in its specific context. But they were established on a few special surfaces and may not be capable to produce satisfying results for an arbitrary part. Besides, they do not consider the simultaneous improvement of the quality of multiple critical surfaces of a part. In this paper, an approach for optimising process parameters to improve the surface quality of laser powder bed fusion parts is proposed. Firstly, Taguchi optimisation is performed to generate a small number of alternative combinations of the process parameters to be optimised. Then, actual build and measurement experiments are conducted to obtain the quality indicator values of a certain number of critical surfaces under each alternative combination. After that, a flexible three-way technique for order of preference by similarity to ideal solution is used to determine the optimal combination of process parameters from the generated alternatives. Finally, a case study is presented to demonstrate the proposed approach. The demonstration results show that the proposed approach only needs a small amount of experimental data and takes into account the simultaneous improvement of the quality of multiple critical surfaces of an arbitrary part.

**Keywords** Process parameter optimisation · Surface roughness · Laser powder bed fusion · Additive manufacturing · Design of experiments · Multi-attribute decision-making

## 1 Introduction

Laser powder bed fusion (LPBF), also known as selective laser melting or direct metal laser melting, is an additive manufacturing (AM) technology utilising a high power-density laser beam to selectively melt and fuse metallic powders together to build near-net-shape parts [1]. This technology has characteristics in providing a high degree of freedom for design and achieving complex geometries without additional cost, which are the common advantages of AM technologies over conventional manufacturing technologies. More importantly, the LPBF technology enables the fabrication of metallic components with near full density and high strength and stiffness. This makes it a very promising metal AM technology for producing functional components in industry [2–6].

Using the LPBF technology to produce a part involves a set of activities, where design is an important one [7]. In this activity, the variables related to material, structure, and process are optimised to improve part quality and to satisfy other lifecycle requirements [8, 9]. Among all optimised variables, process parameters are crucial factors that have an important effect on the quality of produced part [10]. In practice, LPBF part builds generally use certain sets of optimised process parameters empirically developed by the original equipment manufacturers of LPBF systems. Because there are infinite possibilities for part design, functional requirements, and lifecycle considerations, it is not possible to have complete sets of optimised process parameters. This means that using

✉ Shan Lou
s.lou@hud.ac.uk

1 EPSRC Future Advanced Metrology Hub, University of Huddersfield, Huddersfield HD1 3DH, UK

2 Centre for Decision Research, University of Leeds, Leeds LS2 9JT, UK

3 School of Electrical, Electronic and Mechanical Engineering, University of Bristol, Bristol BS8 1QU, UK

the recommended process parameters could produce parts that cannot meet quality requirements [11].

To provide practical process parameter optimisation methods, a lot of studies have been conducted within academia [12, 13]. Many of these studies focus on improving mechanical performance and a few of them consider surface quality. While mechanical properties are critical to part quality, surface quality can also be important in some applications, since it can influence the part accuracy, post-processing, and part functionality. As one example, in aerospace application, a certain surface roughness is required to avoid premature failure from surface-initiated cracking. As another example, in biomedical application, the surface topography with certain roughness can enhance bone-to-implant contact and provide strong bonding capability [14].

Optimisation of process parameters for improving surface quality requires an accurate and efficient prediction model and a robust optimisation method. So far, there have been a number of models for predicting the surface quality of an LPBF part. One of the most common models is an analytical model based on theoretical calculation [15]. In this model, surface roughness is estimated via layer thickness and surface inclination angle. A limitation of the model is that it only considers the staircase effect. Another representative model is an empirical model based on actual measurement [16]. This model was established using the measured roughness data of a set of inclined surfaces, based on which the roughness of a surface with a specific inclination angle is calculated via numerical interpolation. To take advantage of both the analytical and empirical strategies, a few hybrid models were presented in the literature [17–19]. The model in [17] predicts the surface roughness of 316L parts through layer thickness, surface inclination angle, and particle presence. This model is calibrated by the measured roughness data. It not only considers the staircase effect, but also the effect of partially bonded particles on a surface. The model in [18] estimates the surface roughness of Ti6Al4V parts using a linear function, which was established according to an experimental study of the average surface roughness of samples in different build orientations and with a constant layer thickness. The model in [19] predicts the surface roughness of AlSi10Mg parts via staircase effect and defects of the powder used. According to the experimental studies in [20–24], apart from staircase effect, the process parameters to build an LPBF part also have an important influence on the surface quality of the as-built part. However, the existing analytical, empirical, and hybrid models do not consider them in the analysis of surface inclination angle.

In addition to the models above, a category of recently popular models is those based on machine learning [25–31]. Akhil et al. [25] built five mappings from laser power, scanning speed, and hatch spacing to three roughness parameters ($S_a$, $S_q$, and $S_t$), respectively using linear regression, polynomial regression, support vector regression, Gaussian process regression, and artificial neural network. The five models were trained and tested using the surface images of 59 printed Ti6Al4V specimens and the measured roughness parameters of the specimens. The testing and comparison results suggest that the Gaussian process regression model provides the best prediction for all the three roughness parameters. Hertlein et al. [26] related four process parameters and five part quality indicators via a hybrid Bayesian network. The four parameters are layer thickness, laser power, scanning speed, and hatch spacing. The five indicators include density, hardness, top surface roughness, ultimate tensile strength in the build orientation, and ultimate tensile strength perpendicular to the build orientation. The network was trained, validated, and tested using the data collected or converted from 13 publications including physical 316L builds. The testing results show that the model has satisfying accuracy on predicting the hardness and ultimate tensile strength in the build orientation. The accuracy on predicting other indicators is unknown because of limited available data. Fotovvati and Chou [27] established a relationship between four process parameters, including layer thickness, laser power, scanning speed, and hatch spacing, and two roughness parameters ($S_a$ and $S_v$) through an artificial neural network. The network was trained and tested using the data sets constructed from 25 Ti6Al4V samples, which were built under 25 combinations of the four process parameters, and was compared to a linear regression model in terms of mean square error and correlation coefficient. The comparison results suggest that the network outperforms the linear regression model at both aspects. Soler et al. [28] related two manufacturing parameters and seven blasting and electropolishing parameters and the surface roughness of finished parts via an artificial neural network. The network was trained, validated, and tested using 429 historical Ti6Al4V specimens. The model was used to determine the optimal parameters to improve the surface roughness during blasting and electropolishing. Zhang et al. [29] established a relationship between three process parameters, including laser power, scanning speed, and hatch spacing, and top surface roughness through a back propagation neural network. The network was trained and tested using the data obtained from 48 316L samples, which were built under 48 combinations of the three process parameters. La Fé-Perdomo et al. [30] predicted the roughness of the top surfaces of 316L parts using a multilayer perceptron and an adaptive neuro-fuzzy inference system. The input variables of each model include laser power, scanning speed, and hatch spacing. The two models were trained, tested, and compared using the data collected from three publications including physical 316L builds. The comparison results show that the latter model has better accuracy than the former. Maitra et al. [31] built six mappings from seven process parameters to surface roughness, respectively using Gaussian process regression, support vector regression, regression tree, ensemble of trees, neural network, and multiple linear regression. The seven parameters include layer thickness, laser power, scanning speed, hatch spacing, energy density, average particle size, and variance. The six models were trained, tested, and compared using the data collected from 27 publications including physical Ti6Al4V builds. The comparison results show that the Gaussian process regression and neural network models underperform other four models at the aspect of root mean square error. Compared to the analytical, empirical, and hybrid models, machine learning-based models take into account some key process parameters. However, the existing models are trained and tested using the roughness data of the surfaces with specific inclination angles (e.g., top surface, front surface, side surface). They may not be capable to provide accurate prediction results for a surface of an arbitrary part, because the inclination angle of the surface may be different from the inclination angles of the surfaces used for training.

To optimise the process parameters with an objective of improving surface quality, a variety of methods have been developed in the literature [32]. In [33], the influence of remelting parameters for post-processing the surface quality of LPBF parts was investigated. A set of 316L samples with varying inclination angles were printed. Laser re-melting was performed on the samples to investigate surface roughness via optimisation of laser power, scanning speed, and hatch spacing based on statistical analysis within a design of experiments framework. In [34], a set of Ti6Al4V printing experiments were designed to investigate the variance of surface roughness with respect to powder size distribution, powder packing fraction, and process by-product generation. A rational design of experiments was adopted to optimise laser power, scanning speed, and contour offset to improve the quality of inclined surfaces. In [35], the effect of laser power, scanning speed, and hatch spacing on the porosity level, surface roughness, elastic modulus, and compressive strength of Ti6Al4V samples was investigated using response surface methodology. Analysis of variance was applied to optimise the three process parameters. In [36], the relationship between laser power, scanning speed, and hatch spacing and the surface roughness of Ti6Al4V parts was experimentally studied. Response surface methodology was adopted to obtain the optimal process parameters for minimising the roughness of top and vertical side surfaces. In [37], the effect of laser power, scanning speed, overlap rate, and hatch spacing on the front surface roughness and side surface roughness of AlSi10Mg parts was investigated. The influence of laser power was explored empirically. Analysis of variance was adopted to determine the best level of laser power. Regression analysis was carried out to establish a prediction model for optimising scanning speed, overlap rate, and hatch spacing to obtain minimum surface roughness. In [38], response surface methodology was applied to investigate the effect of laser power, scanning speed, and hatch spacing on the relative density and top surface roughness of 316L parts. The quadratic response surface models for relative density and top surface roughness were established based on analysis of variance. A multi-objective collaborative optimisation was performed to optimise the investigated process parameters with respect to relative density and top surface roughness. In [39], a data-driven framework was built to optimise layer thickness, laser power, and scanning speed for improving the surface quality and dimensional accuracy of 316L parts. A Gaussian process regression model was trained to predict top surface roughness and dimensional accuracy. Based on this model, a whale optimisation algorithm was applied to search the optimal combination of the three process parameters. In [40], the effect of laser power and scanning speed on the surface hardness, top surface roughness, and side surface roughness of Ti6Al4V specimens was experimentally studied. Response surface methodology was applied to optimise the two process parameters for improving surface quality. In [41], central composite design was applied to systematically investigate the influence of layer thickness, laser power, scanning speed, and hatch spacing on the relative density and surface roughness of Inconel 718 components. The prediction models for relative density and side surface roughness were built based on response surface methodology and analysis of variance. Based on these models, three multi-objective optimisation methods were developed to simultaneously optimise relative density and surface roughness. In [42], an optimisation framework based on machine learning was established to relate layer thickness, laser power, scanning speed, and hatch spacing and the density ratio and surface roughness of Ti6Al4V components. A deep neural network was trained and applied to recommend the optimal process parameters for maximisation of density ratio and minimisation of top surface roughness. Based on these descriptions, a qualitative comparison of the existing methods is shown in Table 1. As can be seen from the table, the existing methods differ in a number of aspects, which mainly include the applied techniques, experiment material, number of data points, optimised process parameters, and considered responses. There is no doubt that each of these methods can work well in its specific context. It is difficult to conclude that one method is better than others.

**Table 1** A comparison of existing methods to optimise process parameters for improving surface quality

| Method | Techniques | Material | Data points | LT | LP | SS | HS | CO | OR | Responses |
|---|---|---|---|---|---|---|---|---|---|---|
| [33] | DOEs | 316L | 27 | | ✓ | ✓ | ✓ | | | $R_a$ |
| [34] | DOEs | Ti6Al4V | 45 | | ✓ | ✓ | | ✓ | | $R_a$, $R_{sk}$, $R_{\Delta q}$ |
| [35] | RSM, AOV | Ti6Al4V | 17 | | ✓ | ✓ | ✓ | | | $R_a$ |
| [36] | RSM | Ti6Al4V | 20 | | ✓ | ✓ | ✓ | | | $R_a$ |
| [37] | AOV, PR | AlSi10Mg | 81 | | ✓ | ✓ | ✓ | | ✓ | $R_a$ |
| [38] | RSM, AOV, MOO | 316L | 20 | | ✓ | ✓ | ✓ | | | $R_a$ |
| [39] | DOEs, GPR, MOO | 316L | 21 | ✓ | ✓ | ✓ | | | | $R_a$ |
| [40] | RSM | Ti6Al4V | 16 | | ✓ | ✓ | | | | $R_a$ |
| [41] | RSM, AOV, MOO | Inconel 718 | 30 | ✓ | ✓ | ✓ | ✓ | | | $R_a$ |
| [42] | DNN | Ti6Al4V | 2,048 | ✓ | ✓ | ✓ | ✓ | | | $S_a$ |

**Notes**: *LT* layer thickness, *LP* laser power, *SS* scanning speed, *HS* hatch spacing, *CO* contour offset, *OR* overlap rate, *DOEs* design of experiments, *RSM* response surface methodology, *AOV* analysis of variance, *PR* polynomial regression, *MOO* multi-objective optimisation, *GPR* Gaussian process regression, *DNN* deep neural network

However, the methods may not be capable to generate satisfying optimisation results for an arbitrary component, since a component may contain a number of surfaces that have different inclination angles, while the methods were built on a few special surfaces (e.g., top surface, front surface, side surface). In addition, some applications may require simultaneous improvement of the quality of multiple critical surfaces of a part, but the methods do not take this requirement into account.

In this paper, an approach for optimising process parameters to simultaneously improve the quality of multiple critical surfaces of an arbitrary LPBF part is proposed. This method is based on an idea of transforming an infinite solution space into a finite one and selecting the optimal solution from the finite solution space. The transformation and selection are carried out using Taguchi optimisation [43] and a three-way technique for order of preference by similarity to ideal solution (TOPSIS) [44]. Taguchi method is a statistical methodology for finding the minimum number of experiments to be conducted within the permissible limit of factors and levels. In this method, a modified or standard design of experiments is adopted to identify a certain number of parametric combinations of the control factors for improving the quality of manufactured products. The results generated by the Taguchi method may not be optimal, but there is no doubt that product quality can be improved when these results are implemented. The three-way TOPSIS was developed on the basis of TOPSIS [45] and the three-way decision model [46]. TOPSIS is a multi-attribute decision-making (MADM) method that ranks the alternatives according to their geometric distances from the best and worst solutions. It has been widely used in the field of AM because of its simplicity and efficiency [47]. The three-way decision model is a granular computing technique for MADM. It is more flexible and advantageous than traditional MADM methods because it can effectively avoid premature classification of the alternatives at the edge of acceptance and rejection. This feature makes the model very suitable for the MADM problems in metal AM where replacement of inappropriate decisions is costly [48].

The remainder of the paper is organised as follows: Sect. 2 describes the details of the proposed approach. A case study is presented to demonstrate the approach in Sect. 3. Section 4 ends the paper with a conclusion.

## 2 The proposed approach

In this section, the proposed approach for optimising process parameters to improve the surface quality of an LPBF part is described in detail. A general flow of this approach is depicted in Fig. 1. The main process of the approach consists of two stages: optimisation, build, and measurement (OBM) and MADM. In the first stage, a small number of alternative combinations of the process parameters to be optimised for the part and the quality indicator values of a certain number of critical surfaces under each alternative combination are obtained via Taguchi optimisation and actual build and measurement. In the second stage, the optimal combination of process parameters is selected from the obtained alternatives via MADM based on three-way TOPSIS. The details of the two stages are explained below.

### 2.1 Optimisation, build, and measurement

There are three steps in this stage. The first step is to generate a small number of alternative combinations of the process parameters to be optimised for an arbitrary LPBF part. According to the existing experimental studies [20–24], a number of process parameters, mainly including layer thickness, laser power, scanning speed, hatch spacing, point distance, and exposure time, have influence on surface quality. The process parameters to be optimised can be

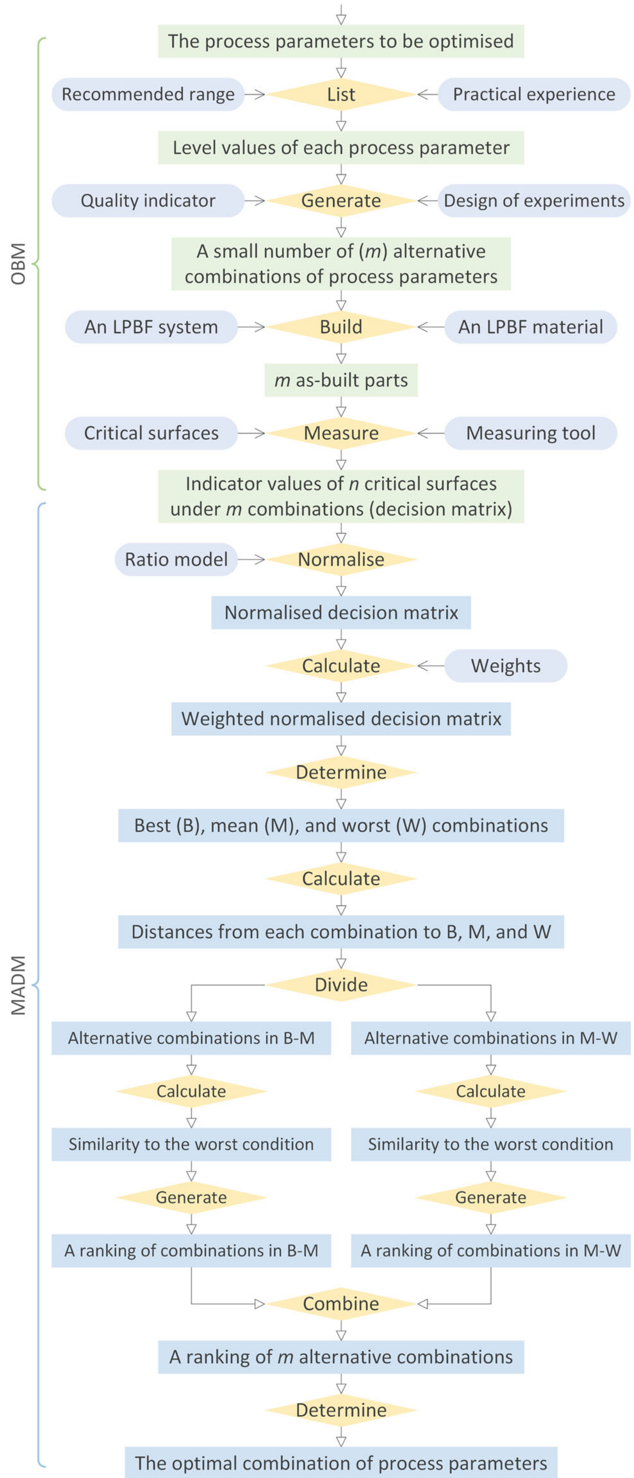


**Fig. 1** A general flow of the proposed approach

determined based on this. In general, each adjustable process parameter for an LPBF system has a specific range recommended by the original equipment manufacturers of the system. Even so, it is still difficult to find a combination of process parameters that will achieve the best surface quality, as there are still infinite possible combinations of process parameters in this case. To deal with this difficulty, the Taguchi method was introduced to generate a small number of alternative combinations of process parameters [43].

According to the Taguchi method, the level values of each process parameter to be optimised are listed based on the recommended range of this parameter and practical experience. Then, a surface quality indicator is selected from a set of parameters (e.g., $R_a$, $S_a$, $S_q$, and $S_t$) defined in the international standards ISO 21920-2:2021 and ISO 25178-2:2021. Design of experiments analysis based on the selected surface quality indicator and a specific orthogonal array is carried out to generate a small number of (let $m$ denote the number) alternative combinations of process parameters. The reason for adopting design of experiments is that it can produce a reduced variance for the experiment process to obtain the best surface quality under the optimal settings of process parameters.

The second step is to conduct an actual build experiment using an LPBF system and an LPBF material. In this experiment, the three-dimensional model of the LPBF part is input to the LPBF system to build $m$ parts under the generated $m$ alternative combinations of process parameters. It is worth noting that apart from the process parameters to be optimised, all other conditions to build the $m$ parts are the same. After the experiment, $m$ as-built parts are obtained.

The third step is to measure the selected quality indicator of specific critical surfaces of each as-built part. The critical surfaces (let $n$ denote their number) are generally identified on the basis of actual functional requirements. Surface quality inspection mainly includes the measurement of profile and areal topographies. Profile topography measurement is generally conducted using a contact stylus. Instruments for areal topography measurement are more diverse, which mainly include focus variation microscopy, conoscopic holography, atomic force microscopy, elastomeric sensor, confocal microscopy, and coherence scanning interferometry [49].

## 2.2 Multi-attribute decision-making

An $m \times n$ data table consisting of $m$ rows and $n$ columns of the measurement data of the selected surface quality indicator is obtained after the first stage. The purpose is to select a combination of process parameters from the $m$ alternatives that can simultaneously optimise the quality of the $n$ critical surfaces. It is obvious that the infinite process parameter optimisation problem is transformed into a finite multi-objective optimisation problem, i.e., an MADM problem. So far, there have been many methods available for solving an MADM problem in the AM domain [47]. This stage adopts a three-way TOPSIS method [44].

Let $C_1, C_2, ..., C_m$ be the $m$ alternative combinations of process parameters, $S_1, S_2, ..., S_n$ be the $n$ critical surfaces, $a_{i,j}$ $(i = 1, 2, ..., m;\ j = 1, 2, ..., n)$ be the value of the quality indicator of $S_j$ under $C_i$, $\boldsymbol{A} = [a_{i,j}]_{m\times n}$ be a decision matrix for the process parameter optimisation problem, and $w_j$ be the weight of $S_j$ such that $0 \le w_j \le 1$ and $\Sigma_{j=1}^{n} w_j = 1$. Using the three-way TOPSIS method, the optimal combination of process parameters can be determined via the following steps:

(1) Normalise the decision matrix. Normalisation of the values of $a_{i,j}$ is required since they are of incongruous dimensions. This can be carried out using the following ratio model:

$$b_{i,j} = \frac{a_{i,j}}{\sqrt{\sum_{i=1}^{m} a_{i,j}^2}} \tag{1}$$

Through the normalisation, a normalised decision matrix is obtained as $\boldsymbol{B} = [b_{i,j}]_{m\times n}$.

(2) Calculate a weighted normalised decision matrix. Based on the normalised decision matrix and the weights of critical surfaces, a weighted normalised decision matrix is established as $\boldsymbol{X} = [X_{i,j}]_{m\times n}$, where $X_{i,j}$ is calculated using the following equation:

$$X_{i,j} = w_j b_{i,j} \tag{2}$$

(3) Determine the best, mean, and worst combinations. Based on the weighted normalised decision matrix, the best, mean, and worst combinations are respectively determined as follows:

$$\begin{aligned}\mathbb{B} &= (Y_{\mathbb{B},1}, Y_{\mathbb{B},2}, ..., Y_{\mathbb{B},n}) \\ &= \left(\left\langle \max_{i=1}^{m} \left\{X_{i,j} \mid j \in J_+\right\}\right\rangle, \left\langle \min_{i=1}^{m} \left\{X_{i,j} \mid j \in J_-\right\}\right\rangle\right)\end{aligned} \tag{3}$$

$$\begin{aligned}\mathbb{M} &= (Y_{\mathbb{M},1}, Y_{\mathbb{M},2}, ..., Y_{\mathbb{M},n}) \\ &= \left(\text{avg}_{i=1}^{m}\left\{X_{i,1}\right\}, \text{avg}_{i=1}^{m}\left\{X_{i,2}\right\}, ..., \text{avg}_{i=1}^{m}\left\{X_{i,n}\right\}\right)\end{aligned} \tag{4}$$

$$\begin{aligned}\mathbb{W} &= (Y_{\mathbb{W},1}, Y_{\mathbb{W},2}, ..., Y_{\mathbb{W},n}) \\ &= \left(\left\langle \min_{i=1}^{m} \left\{X_{i,j} \mid j \in J_+\right\}\right\rangle, \left\langle \max_{i=1}^{m} \left\{X_{i,j} \mid j \in J_-\right\}\right\rangle\right)\end{aligned} \tag{5}$$

where $J_+$ is a set of the subscripts of positive attributes (attributes that have a positive impact on the decision-making result, i.e., the larger their values, the more favourable the decision-making result), $J_-$ is a set of the subscripts of negative attributes (attributes that have a negative impact on the decision-making result, i.e., the smaller their values, the more favourable the decision-making result), and avg is the averaging function.

(4) Calculate the distances from each alternative combination to the best, mean, and worst combinations. According to the Euclidean distance formula, the Euclidean distances between $C_i$ and $\mathbb{B}$, between $C_i$ and $\mathbb{M}$, and between $C_i$ and $\mathbb{W}$ are respectively calculated using the following equations:

$$d(C_i, \mathbb{B}) = \sqrt{\sum_{j=1}^{n} (X_{i,j} - Y_{\mathbb{B},j})^2} \tag{6}$$

$$d(C_i, \mathbb{M}) = \sqrt{\sum_{j=1}^{n} (X_{i,j} - Y_{\mathbb{M},j})^2} \tag{7}$$

$$d(C_i, \mathbb{W}) = \sqrt{\sum_{j=1}^{n} (X_{i,j} - Y_{\mathbb{W},j})^2} \tag{8}$$

(5) Divide the alternative combinations into two segments. For each alternative combination $C_i$, if the number of $X_{i,j}$ such that $X_{i,j} \ge Y_{\mathbb{M},j}$ (when the quality indicator of $S_j$ is a positive attribute) and $X_{i,j} \le Y_{\mathbb{M},j}$ (when the quality indicator of $S_j$ is a negative attribute) is greater than $n/2$, then $C_i$ is classified to a segment $\mathbb{B} - \mathbb{M}$; otherwise, $C_i$ is classified to a segment $\mathbb{M} - \mathbb{W}$. It is obvious that the alternative combinations in $\mathbb{B} - \mathbb{M}$ are superior to the alternative combinations in $\mathbb{M} - \mathbb{W}$.

(6) Calculate the similarity to the worst condition for each alternative combination. If $C_i$ is in $\mathbb{B} - \mathbb{M}$, then the similarity to the worst condition for it is calculated via

$$s_i = \frac{d(C_i, \mathbb{M})}{d(C_i, \mathbb{M}) + d(C_i, \mathbb{B})} \tag{9}$$

If $C_i$ is in $\mathbb{M} - \mathbb{W}$, then the similarity to the worst condition for it is calculated via

$$s_i = \frac{d(C_i, \mathbb{W})}{d(C_i, \mathbb{W}) + d(C_i, \mathbb{M})} \tag{10}$$

(7) Rank the alternative combinations in each segment. The alternative combinations in $\mathbb{B} - \mathbb{M}$ are ranked according to their similarities to the worst condition: The larger the similarity of an alternative combination, the higher its ranking. The alternative combinations in $\mathbb{M} - \mathbb{W}$ are ranked by the same rule.

(8) Obtain a ranking of all alternative combinations. According to the rule that the alternative combinations in $\mathbb{B} - \mathbb{M}$ are superior to the alternative combinations in $\mathbb{M} - \mathbb{W}$, a ranking of all alternative combinations is obtained via combining the ranking results for the two segments.

(9) Determine the optimal combination. According to the obtained ranking, the optimal combination of process parameters is determined.

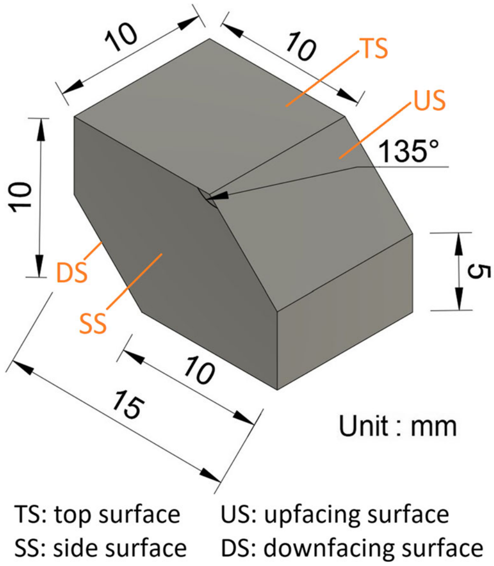


**Fig. 2** A sketch of an LPBF part

## 3 Case study

In this section, a case study extended from [43] is presented to demonstrate the proposed approach. This case study aims to optimise five contour process parameters, including layer thickness, laser power, hatch spacing, point distance, and exposure time, to improve the surface quality of an LPBF part. A sketch of this part is given in Fig. 2. The part will be built using Renishaw AM400 and 316L. According to the proposed approach, the optimisation can be performed below.

According to the ranges of the five process parameters to be optimised recommended by the Renishaw AM400 system and practical experience, the level values of the five process parameters were listed and are shown in Table 2. Then, the roughness parameter $S_a$ was selected to quantify the quality of surfaces and design of experiments analysis based on this parameter, and the orthogonal array of L25 was performed using Minitab 19. The results of this analysis are listed in Table 3, where LT stands for layer thickness, LP stands for laser power, HS stands for hatch spacing, PD stands for point distance, and ET stands for exposure time. Using Renishaw AM400 and 316L stainless steel powder supplied by Renishaw, 25 hexagon parts were built under the generated 25 alternative combinations of process parameters in Table 3. A picture of the 25 as-built parts is given in Fig. 3. The critical surfaces of each part were identified as the top, side, upfacing, and downfacing surfaces. To capture the areal topography of the critical surfaces of each part, Alicona G5 infinite focus variation measurement system was applied. The configurations were a magnification lens of 10×, an illumination type of ring light, a lateral resolution of 2 $\mu$m, a vertical resolution of 1 $\mu$m, a sampling distance of 0.8780 $\mu$m ($x$ and $y$ directions), and a measurement size of 8 mm × 8 mm (stitched). For example, the areal topography of the four critical surfaces of the first as-built part is shown in Figs. 4, 5, 6, and 7, respectively. DigitalSurf MountainMaps was adopted to analyse the surface topographical data. Only levelling was applied, and no other filtration operations were performed to avoid losing surface information. The analysed data was used to generate the $S_a$ values of the four critical surfaces of the 25 as-built parts. The results are also listed in Table 3, where TS stands for top surface, SS stands for side surface, US stands for upfacing surface, and DS stands for downfacing surface.

**Table 2** Level (L) values of the process parameters to be optimised

| Process parameters | L1 | L2 | L3 | L4 | L5 |
|---|---|---|---|---|---|
| Layer thickness ($\mu$m) | 25 | 50 | 75 | 100 | 125 |
| Laser power (W) | 90 | 120 | 150 | 180 | 210 |
| Hatch spacing ($\mu$m) | 30 | 60 | 90 | 120 | 150 |
| Point distance ($\mu$m) | 25 | 50 | 75 | 100 | 125 |
| Exposure time ($\mu$s) | 30 | 60 | 90 | 120 | 150 |

Now, the infinite process parameter optimisation problem is transformed into an MADM problem, which aims to select a combination of process parameters that can simultaneously minimise the $S_a$ values of the four critical surfaces from the 25 alternatives. Let $C_1$, $C_2$, ..., $C_{25}$ be the 25 alternative combinations of process parameters, $S_1$, $S_2$, $S_3$, and $S_4$ be the four critical surfaces, $a_{i,j}$ ($i = 1, 2, ..., 25$; $j = 1, 2, 3, 4$) be the $S_a$ value of $S_j$ under $C_i$, $\boldsymbol{A} = [a_{i,j}]_{25\times4}$ be a decision matrix for the process parameter optimisation problem whose elements are listed in Table 3, and $w_j$ be the weight of $S_j$ such that $0 \leq w_j \leq 1$ and $\Sigma_{j=1}^{n} w_j = 1$. Assume $[w_1, w_2, w_3, w_4] = [0.2, 0.2, 0.3, 0.3]$. Then, the optimal combination of process parameters is determined through the following steps:

(1) Normalise the decision matrix. According to the ratio model in Eq. (1), the decision matrix $\boldsymbol{A}$ is normalised and a normalised decision matrix is obtained as $\boldsymbol{B} = [b_{i,j}]_{25\times4}$, where the values of $b_{i,j}$ are listed in Table 4.
(2) Calculate a weighted normalised decision matrix. According to the normalised decision matrix, the given weights, and Eq. (2), a weighted normalised decision matrix is established as $\boldsymbol{X} = [X_{i,j}]_{25\times4}$, where the values of $X_{i,j}$ are also listed in Table 4.
(3) Determine the best, mean, and worst combinations. Based on the weighted normalised decision matrix, the best, mean, and worst combinations are respectively determined as $\mathbb{B} = (0.0087, 0.0190, 0.0111, 0.0339)$,

**Table 3** Results of design of experiments analysis and actual measurements

| No $C_i$ | LT ($\mu$m) | LP (W) | HS ($\mu$m) | PD ($\mu$m) | ET ($\mu$s) | TS $S_a$ ($\mu$m) | SS $S_a$ ($\mu$m) | US $S_a$ ($\mu$m) | DS $S_a$ ($\mu$m) |
|---|---|---|---|---|---|---|---|---|---|
| 1 | 30 | 100 | 25 | 20 | 40 | 191.7 | 20.9 | 94.1 | 68.3 |
| 2 | 60 | 100 | 50 | 40 | 80 | 45.7 | 12.0 | 37.1 | 43.7 |
| 3 | 90 | 100 | 75 | 60 | 120 | 24.3 | 15.0 | 25.8 | 34.5 |
| 4 | 120 | 100 | 100 | 80 | 160 | 36.0 | 19.6 | 32.2 | 34.8 |
| 5 | 150 | 100 | 125 | 100 | 200 | 47.4 | 26.4 | 41.4 | 48.2 |
| 6 | 120 | 125 | 25 | 40 | 120 | 165.2 | 19.3 | 78.1 | 131.0 |
| 7 | 150 | 125 | 50 | 60 | 160 | 73.5 | 23.0 | 43.5 | 49.2 |
| 8 | 30 | 125 | 75 | 80 | 200 | 81.3 | 8.8 | 14.2 | 40.0 |
| 9 | 60 | 125 | 100 | 100 | 40 | 20.1 | 15.6 | 27.1 | 34.3 |
| 10 | 90 | 125 | 125 | 20 | 80 | 39.5 | 10.1 | 17.9 | 34.7 |
| 11 | 60 | 150 | 25 | 60 | 200 | 239.5 | 9.0 | 97.4 | 108.9 |
| 12 | 90 | 150 | 50 | 80 | 40 | 37.7 | 14.6 | 51.0 | 55.9 |
| 13 | 120 | 150 | 75 | 100 | 80 | 65.9 | 21.1 | 31.7 | 41.6 |
| 14 | 150 | 150 | 100 | 20 | 120 | 38.7 | 13.2 | 26.3 | 47.8 |
| 15 | 30 | 150 | 125 | 40 | 160 | 46.9 | 8.0 | 10.4 | 34.4 |
| 16 | 150 | 175 | 25 | 80 | 80 | 124.6 | 20.1 | 65.4 | 92.6 |
| 17 | 30 | 175 | 50 | 100 | 120 | 46.6 | 12.7 | 11.9 | 35.1 |
| 18 | 60 | 175 | 75 | 20 | 160 | 27.9 | 10.3 | 13.2 | 35.9 |
| 19 | 90 | 175 | 100 | 40 | 200 | 27.6 | 9.7 | 14.7 | 34.5 |
| 20 | 120 | 175 | 125 | 60 | 40 | 62.1 | 26.9 | 34.7 | 42.5 |
| 21 | 90 | 200 | 25 | 100 | 160 | 168.8 | 13.7 | 106.1 | 127.6 |
| 22 | 120 | 200 | 50 | 20 | 200 | 62.3 | 14.0 | 21.5 | 45.7 |
| 23 | 150 | 200 | 75 | 40 | 40 | 68.7 | 29.7 | 37.9 | 43.9 |
| 24 | 30 | 200 | 100 | 60 | 80 | 46.8 | 9.6 | 8.8 | 34.4 |
| 25 | 60 | 200 | 125 | 80 | 120 | 29.4 | 8.2 | 15.0 | 36.5 |

$\mathbb{M} = (0.0314, 0.0372, 0.0484, 0.0529)$, and $\mathbb{W} = (0.1035, 0.0705, 0.1342, 0.1296)$.

(4) Calculate the distances from each alternative combination to the best, mean, and worst combinations. According to Eqs. (6), (7), and (8), the Euclidean distances between $C_i$ and $\mathbb{B}$, between $C_i$ and $\mathbb{M}$, and between $C_i$ and $\mathbb{W}$ are respectively calculated and listed in Table 5.

(5) Divide the alternative combinations into two segments. According to the classification rules, the 25 alternative combinations are divided into two segments $\mathbb{B}-\mathbb{M} = \{C_2, C_3, C_4, C_8, C_9, C_{10}, C_{13}, C_{14}, C_{15}, C_{17}, C_{18}, C_{19}, C_{20}, C_{22}, C_{23}, C_{24}, C_{25}\}$ and $\mathbb{M}-\mathbb{W} = \{C_1, C_5, C_6, C_7, C_{11}, C_{12}, C_{16}, C_{21}\}$.

(6) Calculate the similarity to the worst condition for each alternative combination. According to Eqs. (9) or (10),

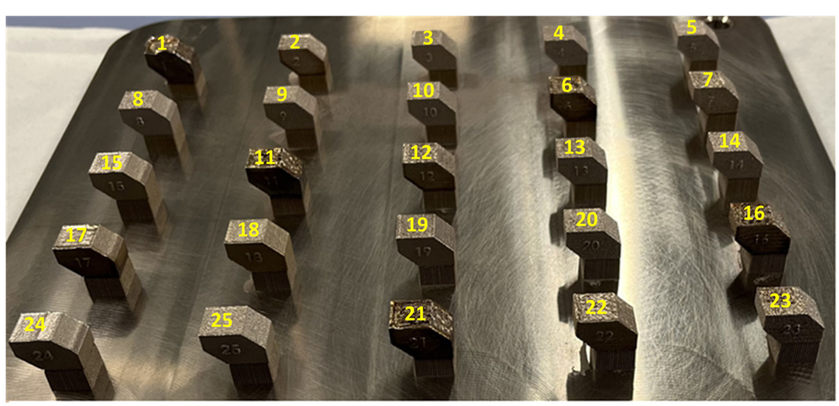


**Fig. 3** A picture of the 25 as-built LPBF parts

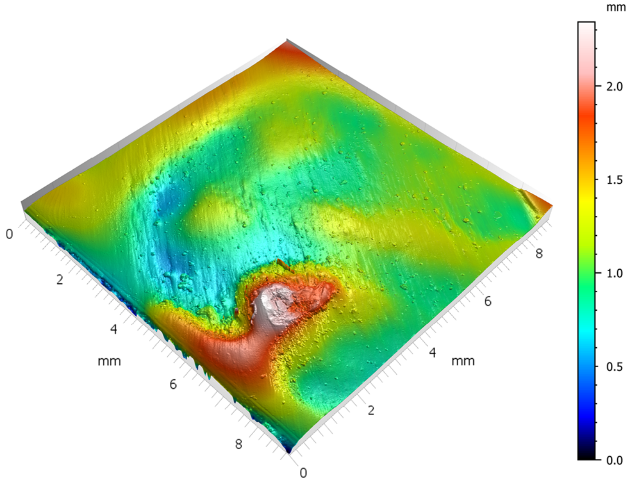


Fig. 4 Areal topography of the top surface of the first as-built part

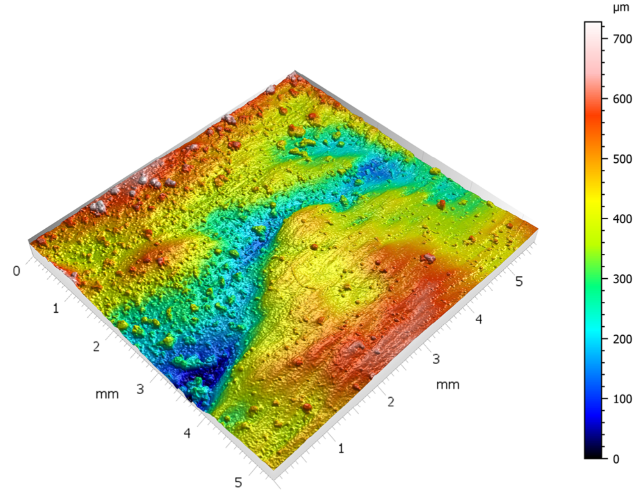


Fig. 6 Areal topography of the upfacing surface of the first as-built part

the similarity to the worst condition for each alternative combination is respectively calculated and also listed in Table 5.

(7) Rank the alternative combinations in each segment. According to the ranking rule, the alternative combinations in $\mathbb{B}-\mathbb{M}$ and $\mathbb{M}-\mathbb{W}$ are ranked as $C_{18} \succ C_{19} \succ C_{25} \succ C_{15} \succ C_{24} \succ C_{10} \succ C_{17} \succ C_8 \succ C_3 \succ C_9 \succ C_{22} \succ C_{14} \succ C_4 \succ C_{23} \succ C_{20} \succ C_2 \succ C_{13}$ and $C_7 \succ C_{12} \succ C_5 \succ C_{16} \succ C_1 \succ C_6 \succ C_{11} \succ C_{21}$, respectively.

(8) Obtain a ranking of all alternative combinations. Through combining the two rankings, a ranking of all alternative combinations is obtained as $C_{18} \succ C_{19} \succ C_{25} \succ C_{15} \succ C_{24} \succ C_{10} \succ C_{17} \succ C_8 \succ C_3 \succ C_9 \succ C_{22} \succ C_{14} \succ C_4 \succ C_{23} \succ C_{20} \succ C_2 \succ C_{13} \succ C_7 \succ C_{12} \succ C_5 \succ C_{16} \succ C_1 \succ C_6 \succ C_{11} \succ C_{21}$.

(9) Determine the optimal combination. According to the obtained ranking, the optimal combination of process parameters is determined as $C_{18}$, which corresponds to a layer thickness of 60 $\mu$m, a laser power of 175 W, a hatch spacing of 75 $\mu$m, a point distance of 20 $\mu$m, and an exposure time of 160 $\mu$s.

## 4 Conclusion

In this paper, an approach for optimising process parameters to improve the surface quality of an LPBF part is presented. The main process of this approach consists of an OBM

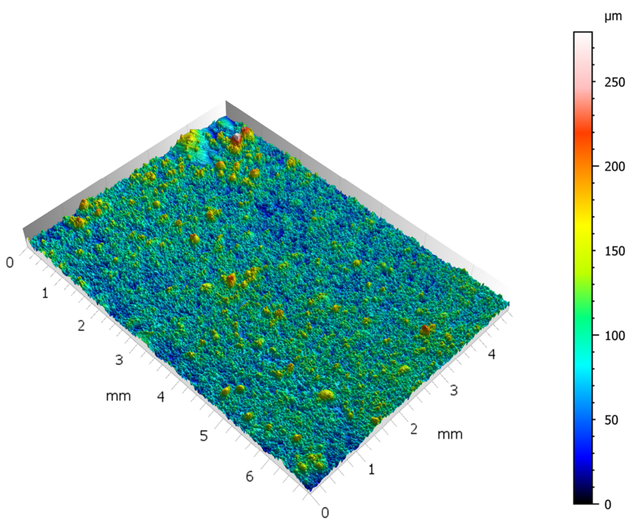


Fig. 5 Areal topography of the side surface of the first as-built part

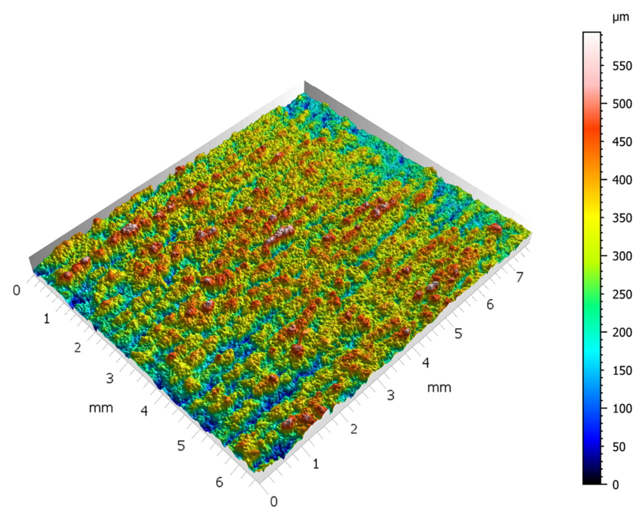


Fig. 7 Areal topography of the downfacing surface of the first as-built part

**Table 4** Elements of the normalised decision matrix and weighted normalised decision matrix

| $C_i$ | $b_{i,1}$ | $b_{i,2}$ | $b_{i,3}$ | $b_{i,4}$ | $X_{i,1}$ | $X_{i,2}$ | $X_{i,3}$ | $X_{i,4}$ |
|---|---|---|---|---|---|---|---|---|
| 1 | 0.4141 | 0.2480 | 0.3967 | 0.2252 | 0.0828 | 0.0496 | 0.1190 | 0.0676 |
| 2 | 0.0987 | 0.1424 | 0.1564 | 0.1441 | 0.0197 | 0.0285 | 0.0469 | 0.0432 |
| 3 | 0.0525 | 0.1780 | 0.1088 | 0.1138 | 0.0105 | 0.0356 | 0.0326 | 0.0341 |
| 4 | 0.0778 | 0.2326 | 0.1358 | 0.1148 | 0.0156 | 0.0465 | 0.0407 | 0.0344 |
| 5 | 0.1024 | 0.3132 | 0.1745 | 0.1590 | 0.0205 | 0.0626 | 0.0524 | 0.0477 |
| 6 | 0.3569 | 0.2290 | 0.3293 | 0.4320 | 0.0714 | 0.0458 | 0.0988 | 0.1296 |
| 7 | 0.1588 | 0.2729 | 0.1834 | 0.1623 | 0.0318 | 0.0546 | 0.0550 | 0.0487 |
| 8 | 0.1756 | 0.1044 | 0.0599 | 0.1319 | 0.0351 | 0.0209 | 0.0180 | 0.0396 |
| 9 | 0.0434 | 0.1851 | 0.1143 | 0.1131 | 0.0087 | 0.0370 | 0.0343 | 0.0339 |
| 10 | 0.0853 | 0.1198 | 0.0755 | 0.1144 | 0.0171 | 0.0240 | 0.0226 | 0.0343 |
| 11 | 0.5174 | 0.1068 | 0.4106 | 0.3591 | 0.1035 | 0.0214 | 0.1232 | 0.1077 |
| 12 | 0.0814 | 0.1732 | 0.2150 | 0.1843 | 0.0163 | 0.0346 | 0.0645 | 0.0553 |
| 13 | 0.1424 | 0.2504 | 0.1336 | 0.1372 | 0.0285 | 0.0501 | 0.0401 | 0.0412 |
| 14 | 0.0836 | 0.1566 | 0.1109 | 0.1576 | 0.0167 | 0.0313 | 0.0333 | 0.0473 |
| 15 | 0.1013 | 0.0949 | 0.0438 | 0.1134 | 0.0203 | 0.0190 | 0.0132 | 0.0340 |
| 16 | 0.2692 | 0.2385 | 0.2757 | 0.3054 | 0.0538 | 0.0477 | 0.0827 | 0.0916 |
| 17 | 0.1007 | 0.1507 | 0.0502 | 0.1158 | 0.0201 | 0.0301 | 0.0151 | 0.0347 |
| 18 | 0.0603 | 0.1222 | 0.0557 | 0.1184 | 0.0121 | 0.0244 | 0.0167 | 0.0355 |
| 19 | 0.0596 | 0.1151 | 0.0620 | 0.1138 | 0.0119 | 0.0230 | 0.0186 | 0.0341 |
| 20 | 0.1341 | 0.3192 | 0.1463 | 0.1402 | 0.0268 | 0.0638 | 0.0439 | 0.0420 |
| 21 | 0.3646 | 0.1626 | 0.4473 | 0.4208 | 0.0729 | 0.0325 | 0.1342 | 0.1262 |
| 22 | 0.1346 | 0.1661 | 0.0906 | 0.1507 | 0.0269 | 0.0332 | 0.0272 | 0.0452 |
| 23 | 0.1484 | 0.3524 | 0.1598 | 0.1448 | 0.0297 | 0.0705 | 0.0479 | 0.0434 |
| 24 | 0.1011 | 0.1139 | 0.0371 | 0.1134 | 0.0202 | 0.0228 | 0.0111 | 0.0340 |
| 25 | 0.0635 | 0.0973 | 0.0632 | 0.1204 | 0.0127 | 0.0195 | 0.0190 | 0.0361 |

**Table 5** Distances, segments, and similarities

| $C_i$ | $d(C_i, \mathbb{B})$ | $d(C_i, \mathbb{M})$ | $d(C_i, \mathbb{W})$ | Segment | $s_i$ |
|---|---|---|---|---|---|
| 2 | 0.0398 | 0.0175 | 0.1544 | $\mathbb{B}-\mathbb{M}$ | 0.3059 |
| 3 | 0.0272 | 0.0323 | 0.1711 | $\mathbb{B}-\mathbb{M}$ | 0.5423 |
| 4 | 0.0410 | 0.0272 | 0.1616 | $\mathbb{B}-\mathbb{M}$ | 0.3986 |
| 8 | 0.0279 | 0.0372 | 0.1696 | $\mathbb{B}-\mathbb{M}$ | 0.5710 |
| 9 | 0.0293 | 0.0328 | 0.1710 | $\mathbb{B}-\mathbb{M}$ | 0.5278 |
| 10 | 0.0151 | 0.0373 | 0.1765 | $\mathbb{B}-\mathbb{M}$ | 0.7118 |
| 13 | 0.0474 | 0.0195 | 0.1507 | $\mathbb{B}-\mathbb{M}$ | 0.2919 |
| 14 | 0.0298 | 0.0226 | 0.1613 | $\mathbb{B}-\mathbb{M}$ | 0.4319 |
| 15 | 0.0118 | 0.0453 | 0.1826 | $\mathbb{B}-\mathbb{M}$ | 0.7941 |
| 17 | 0.0165 | 0.0403 | 0.1782 | $\mathbb{B}-\mathbb{M}$ | 0.7096 |
| 18 | 0.0086 | 0.0430 | 0.1820 | $\mathbb{B}-\mathbb{M}$ | 0.8326 |
| 19 | 0.0091 | 0.0427 | 0.1820 | $\mathbb{B}-\mathbb{M}$ | 0.8245 |
| 20 | 0.0590 | 0.0295 | 0.1474 | $\mathbb{B}-\mathbb{M}$ | 0.3334 |
| 22 | 0.0303 | 0.0234 | 0.1607 | $\mathbb{B}-\mathbb{M}$ | 0.4350 |
| 23 | 0.0674 | 0.0347 | 0.1425 | $\mathbb{B}-\mathbb{M}$ | 0.3398 |
| 24 | 0.0121 | 0.0456 | 0.1830 | $\mathbb{B}-\mathbb{M}$ | 0.7897 |
| 25 | 0.0091 | 0.0426 | 0.1813 | $\mathbb{B}-\mathbb{M}$ | 0.8241 |
| 1 | 0.1386 | 0.0894 | 0.0703 | $\mathbb{M}-\mathbb{W}$ | 0.4401 |

**Table 5** continued

| $C_i$ | $d(C_i, \mathbb{B})$ | $d(C_i, \mathbb{M})$ | $d(C_i, \mathbb{W})$ | Segment | $s_i$ |
|---|---|---|---|---|---|
| 5 | 0.0627 | 0.0285 | 0.1427 | $\mathbb{M}-\mathbb{W}$ | 0.8336 |
| 6 | 0.1466 | 0.1005 | 0.0538 | $\mathbb{M}-\mathbb{W}$ | 0.3487 |
| 7 | 0.0628 | 0.0191 | 0.1350 | $\mathbb{M}-\mathbb{W}$ | 0.8761 |
| 11 | 0.1643 | 0.1185 | 0.0549 | $\mathbb{M}-\mathbb{W}$ | 0.3166 |
| 12 | 0.0601 | 0.0223 | 0.1388 | $\mathbb{M}-\mathbb{W}$ | 0.8613 |
| 16 | 0.1064 | 0.0574 | 0.0841 | $\mathbb{M}-\mathbb{W}$ | 0.5946 |
| 21 | 0.1673 | 0.1203 | 0.0488 | $\mathbb{M}-\mathbb{W}$ | 0.2887 |

stage and an MADM stage. In the OBM stage, design of experiments analysis, build experiments, and measurement experiments are successively conducted to obtain a certain number of alternative combinations of the process parameters to be optimised for an LPBF part and quality indicator values of critical surfaces of the part under each alternative combination. In the MADM stage, a three-way TOPSIS is adopted to select the optimal combination of process parameters from the obtained alternatives. The paper also introduces a case study to demonstrate the presented approach.

A main feature of the presented approach is that it requires a small amount of experimental data and considers the simultaneous improvement of the quality of multiple critical surfaces of an arbitrary part. As described in the introduction, many existing approaches are based on machine learning. They generally need a large amount of experimental data to achieve satisfying results. Compared to these approaches, the presented approach only requires the experimental data under a small number of alternative combinations of process parameters. In addition, the existing approaches may not be capable to generate satisfying results for an arbitrary part and do not consider the simultaneous improvement of the quality of multiple critical surfaces, while the presented approach is free of such limitations. Of course, the shortcoming of the presented approach is easy to imagine. That is, the quality of its optimal solution may be worse than that of the existing approaches based on machine learning. To this end, an approach based on machine learning is preferred when the experimental data is sufficient. Otherwise, the presented approach can be a candidate.

Future work will be devoted to extending the presented approach by adding optimisation of build orientation. The authors have conducted studies on characterising the surface topography of an LPBF part [50], analysing the status of build orientation optimisation [51], investigating the impact of build orientations on the resultant surface textures of an LPBF part [52], and optimising build orientation to reduce the surface roughness of an LPBF part [53, 54]. In the next step, a combination of these studies and the presented approach to simultaneously optimise build orientation and process parameters to improve the surface quality of an LPBF part will be considered. Further, it would be of necessity to include improvement of the mechanical properties of an LPBF part to the presented approach, as both surface quality and mechanical properties are critical to part performance.

**Funding** This study was supported by the National Natural Science Foundation of China (no. 52105511), EPSRC New Investigator Award (Ref. EP/S000453/1), and 3M Buckley Innovation Centre via a 3M BIC Fellowship.

## Declarations

**Ethical approval** This paper does not contain any studies with human participants or animals performed by any of the authors.

**Competing interests** The authors declare no competing interests.

**Open Access** This article is licensed under a Creative Commons Attribution 4.0 International License, which permits use, sharing, adaptation, distribution and reproduction in any medium or format, as long as you give appropriate credit to the original author(s) and the source, provide a link to the Creative Commons licence, and indicate if changes were made. The images or other third party material in this article are included in the article's Creative Commons licence, unless indicated otherwise in a credit line to the material. If material is not included in the article's Creative Commons licence and your intended use is not permitted by statutory regulation or exceeds the permitted use, you will need to obtain permission directly from the copyright holder. To view a copy of this licence, visit http://creativecommons.org/licenses/by/4.0/.

## References

1. Gibson I, Rosen D, Stucker B (2015) Additive manufacturing technologies: 3D printing, rapid prototyping, and direct digital manufacturing, 2nd edn. Springer, New York
2. Sing SL, Yeong WY (2020) Laser powder bed fusion for metal additive manufacturing: perspectives on recent developments. Virtual Phys Prototyp. 15(3):359–70
3. Gu D, Shi X, Poprawe R, Bourell DL, Setchi R, Zhu J (2021) Material-structure-performance integrated laser-metal additive manufacturing. Science 372(6545):eabg1487
4. Han T, Liu Y, Yang D, Qu N, Liao M, Lai Z et al (2022) Effect of annealing on microstructure and mechanical properties of AlCrFe2Ni2 medium entropy alloy fabricated by laser powder bed fusion additive manufacturing. Mater Sci Eng A 839:142868

5. Liang J, Wu S, Li B, Lei Z, Chen Y, Jiang M et al (2023) Microstructure and corrosion behavior of Y-modified ZK60 Mg alloy prepared by laser powder bed fusion. Corros Sci 211:110895
6. Han T, Chen J, Wei Z, Qu N, Liu Y, Yang D et al (2023) Effect of cooling rate on microstructure and mechanical properties of AlCrFe2Ni2 medium entropy alloy fabricated by laser powder bed fusion. J Mater Res Technol 25:4063–73
7. Qin Y, Qi Q, Scott PJ, Jiang X (2019) Status, comparison, and future of the representations of additive manufacturing data. Comput Aided Des 111:44–64
8. Thompson MK, Moroni G, Vaneker T, Fadel G, Campbell RI, Gibson I et al (2016) Design for additive manufacturing: trends, opportunities, considerations, and constraints. CIRP Annals 65(2):737–60
9. Vaneker T, Bernard A, Moroni G, Gibson I, Zhang Y (2020) Design for additive manufacturing: framework and methodology. CIRP Annals 69(2):578–99
10. Khorasani A, Gibson I, Awan US, Ghaderi A (2019) The effect of SLM process parameters on density, hardness, tensile strength and surface quality of Ti-6Al-4V. Addit Manuf 25:176–86
11. Oliveira JP, LaLonde AD, Ma J (2020) Processing parameters in laser powder bed fusion metal additive manufacturing. Materials & Design 193:108762
12. Shipley H, McDonnell D, Culleton M, Coull R, Lupoi R, O'Donnell G et al (2018) Optimisation of process parameters to address fundamental challenges during selective laser melting of Ti-6Al-4V: a review. Int J Mach Tools Manuf 128:1–20
13. Ahmed N, Barsoum I, Haidemenopoulos G, Al-Rub RA (2022) Process parameter selection and optimization of laser powder bed fusion for 316L stainless steel: A review. J Manuf Process 75:415–34
14. Rott S, Ladewig A, Friedberger K, Casper J, Full M, Schleifenbaum JH (2020) Surface roughness in laser powder bed fusion-Interdependency of surface orientation and laser incidence. Addit Manuf 36:101437
15. Campbell RI, Martorelli M, Lee HS (2002) Surface roughness visualisation for rapid prototyping models. Comput Aided Des 34(10):717–25
16. Ahn D, Kim H, Lee S (2009) Surface roughness prediction using measured data and interpolation in layered manufacturing. J Mater Process Technol 209(2):664–71
17. Strano G, Hao L, Everson RM, Evans KE (2013) Surface roughness analysis, modelling and prediction in selective laser melting. J Mater Process Technol 213(4):589–97
18. Brika SE, Zhao YF, Brochu M, Mezzetta J (2017) Multi-objective build orientation optimization for powder bed fusion by laser. J Manuf Sci Eng 139(11):111011
19. Boschetto A, Bottini L, Veniali F (2017) Roughness modeling of AlSi10Mg parts fabricated by selective laser melting. J Mater Process Technol 241:154–63
20. Wang D, Liu Y, Yang Y, Xiao D (2016) Theoretical and experimental study on surface roughness of 316L stainless steel metal parts obtained through selective laser melting. Rapid Prototyp J 22(4):706–16
21. Tian Y, Tomus D, Rometsch P, Wu X (2017) Influences of processing parameters on surface roughness of Hastelloy X produced by selective laser melting. Addit Manuf 13:103–12
22. Calignano F (2018) Investigation of the accuracy and roughness in the laser powder bed fusion process. Virtual Phys Prototyp 13(2):97–104
23. Whip B, Sheridan L, Gockel J (2019) The effect of primary processing parameters on surface roughness in laser powder bed additive manufacturing. Int J Adv Manuf Technol 103:4411–22
24. Zhu Z, Lou S, Majewski C (2020) Characterisation and correlation of areal surface texture with processing parameters and porosity of high speed sintered parts. Addit Manuf 36:101402
25. Akhil V, Raghav G, Arunachalam N, Srinivas DS (2020) Image data-based surface texture characterization and prediction using machine learning approaches for additive manufacturing. J Comput Inf Sci Eng 20(2):021010
26. Hertlein N, Deshpande S, Venugopal V, Kumar M, Anand S (2020) Prediction of selective laser melting part quality using hybrid Bayesian network. Addit Manuf 32:101089
27. Fotovvati B, Chou K (2022) Build surface study of single-layer raster scanning in selective laser melting: surface roughness prediction using deep learning. Manufa Lett 33:701–11
28. Soler D, Telleria M, García-Blanco MB, Espinosa E, Cuesta M, Arrazola PJ (2022) Prediction of surface roughness of SLM built parts after finishing processes using an artificial neural network. J Manuf Mater Process 6(4):82
29. Zhang W, Luo C, Ma Q, Lin Z, Yang L, Zheng J, et al (2022) Prediction model of surface roughness of selective laser melting formed parts based on back propagation neural network. Engineering Reports
30. La Fé-Perdomo I, Ramos-Grez J, Mujica R, Rivas M (2023) Surface roughness Ra prediction in selective laser melting of 316L stainless steel by means of artificial intelligence inference. J King Saud Univ Eng Sci 35(2):148–56
31. Maitra V, Shi J (2023) Evaluating the predictability of surface roughness of Ti-6Al-4V alloy from selective laser melting. Adv Eng Mater 2300075:1–17
32. Hashmi AW, Mali HS, Meena A (2023) A comprehensive review on surface quality improvement methods for additively manufactured parts. Rapid Prototyp J 29(3):504–57
33. Alrbaey K, Wimpenny D, Tosi R, Manning W, Moroz A (2014) On optimization of surface roughness of selective laser melted stainless steel parts: a statistical study. J Mater Eng Perform 23:2139–48
34. Chen Z, Wu X, Tomus D, Davies CH (2018) Surface roughness of selective laser melted Ti-6Al-4V alloy components. Additive Manufacturing 21:91–103
35. Elsayed M, Ghazy M, Youssef Y, Essa K (2018) Optimization of SLM process parameters for Ti6Al4V medical implants. Rapid Prototyp J 25(3):433–47
36. Li Z, Kucukkoc I, Zhang DZ, Liu F (2018) Optimising the process parameters of selective laser melting for the fabrication of Ti6Al4V alloy. Rapid Prototyp J 24(1):150–9
37. Majeed A, Ahmed A, Salam A, Sheikh MZ (2019) Surface quality improvement by parameters analysis, optimization and heat treatment of AlSi10Mg parts manufactured by SLM additive manufacturing. Int J Lightweight Mater Manuf 2(4):288–95
38. Deng Y, Mao Z, Yang N, Niu X, Lu X (2020) Collaborative optimization of density and surface roughness of 316L stainless steel in selective laser melting. Materials 13(7):1601
39. Cao L, Li J, Hu J, Liu H, Wu Y, Zhou Q (2021) Optimization of surface roughness and dimensional accuracy in LPBF additive manufacturing. Optics & Laser Technology. 142:107246
40. Oyesola M, Mpofu K, Mathe N, Fatoba S, Hoosain S, Daniyan I (2021) Optimization of selective laser melting process parameters for surface quality performance of the fabricated Ti6Al4V. Int J Adv Manuf Technol 114:1585–99
41. Lu C, Shi J (2022) Relative density and surface roughness prediction for Inconel 718 by selective laser melting: central composite design and multi-objective optimization. Int J Adv Manuf Technol 119:3931–49
42. Park HS, Nguyen DS, Le-Hong T, Van Tran X (2022) Machine learning-based optimization of process parameters in selective laser melting for biomedical applications. J Intell Manuf 33(6):1843-58
43. Narasimharaju SR, Liu W, Zeng W, Scott P, Jiang J, Lou S (2022) Influence of critical process parameters on surface roughness and statistical optimization of LPBF 316L stainless steel. In: 2022 Summer tropical meeting: advancing precision in additive man-

ufacturing, vol 77. American Society for Precision Engineering, pp 113–8
44. Wang Y, Liu P, Yao Y (2022) BMW-TOPSIS: a generalized TOPSIS model based on three-way decision. Inf Sci 607:799–818
45. Hwang CL, Yoon K (1981) Multiple attribute decision making: methods and applications a state-of-the-art survey. Springer, Berlin
46. Yao Y (2010) Three-way decisions with probabilistic rough sets. Inf Sci 180(3):341–53
47. Qin Y, Qi Q, Shi P, Lou S, Scott PJ, Jiang X (2023) Multi-attribute decision-making methods in additive manufacturing: the state of the art. Processes 11(2):497
48. Qin Y, Qi Q, Shi P, Scott PJ, Jiang X (2023) Selection of materials in metal additive manufacturing via three-way decision-making. Int J Adv Manuf Technol 126(3–4):1293–302
49. Townsend A, Senin N, Blunt L, Leach RK, Taylor JS (2016) Surface texture metrology for metal additive manufacturing: a review. Precis Eng 46:34–47
50. Lou S, Jiang X, Sun W, Zeng W, Pagani L, Scott PJ (2019) Characterisation methods for powder bed fusion processed surface topography. Precis Eng 57:1–15
51. Qin Y, Qi Q, Shi P, Scott PJ, Jiang X (2021) Status, issues, and future of computer-aided part orientation for additive manufacturing. Int J Adv Manuf Technol 115(5–6):1295–328
52. Narasimharaju SR, Liu W, Zeng W, See TL, Scott P, Jiang X et al (2021) Surface texture characterization of metal selective laser melted part with varying surface inclinations. J Tribol 143(5):051106
53. Qin Y, Qi Q, Shi P, Scott PJ, Jiang X (2020) Automatic generation of alternative build orientations for laser powder bed fusion based on facet clustering. Virtual Phys Prototyp 15(3):307–24
54. Qin Y, Qi Q, Shi P, Scott PJ, Jiang X (2021) Automatic determination of part build orientation for laser powder bed fusion. Virtual Phys Prototyp 16(1):29–49

**Publisher's Note** Springer Nature remains neutral with regard to jurisdictional claims in published maps and institutional affiliations.